



Kinetics of the reaction between hydrogen peroxide and aqueous iodine: Implications for technical and natural aquatic systems

Jaedon Shin ^{a, b}, Yunho Lee ^b, Urs von Gunten ^{a, c, d, *}

^a School of Architecture, Civil and Environmental Engineering (ENAC), École Polytechnique Fédérale de Lausanne (EPFL), CH-1015, Lausanne, Switzerland

^b School of Earth Sciences and Environmental Engineering, Gwangju Institute of Science and Technology (GIST), Gwangju, 61005, Republic of Korea

^c Eawag, Swiss Federal Institute of Aquatic Science and Technology, Ueberlandstrasse 133, CH-8600, Dübendorf, Switzerland

^d Institute of Biogeochemistry and Pollutant Dynamics, ETH Zurich, 8092, Zurich, Switzerland

ARTICLE INFO

Article history:

Received 2 March 2020

Received in revised form

16 April 2020

Accepted 17 April 2020

Available online 23 April 2020

Keywords:

Hydrogen peroxide

Hypoiodous acid

Iodide

Oxidation

Disinfection byproducts

Ozone deposition

ABSTRACT

Oxidative treatment of iodide-containing waters can lead to a formation of potentially toxic iodinated disinfection byproducts (I-DBPs). Iodide (I^-) is easily oxidized to HOI by various oxidation processes and its reaction with dissolved organic matter (DOM) can produce I-DBPs. Hydrogen peroxide (H_2O_2) plays a key role in minimizing the formation of I-DBPs by reduction of HOI during H_2O_2 -based advanced oxidation processes or water treatment based on peracetic acid or ferrate(VI). To assess the importance of these reactions, second order rate constants for the reaction of HOI with H_2O_2 were determined in the pH range of 4.0–12.0. H_2O_2 showed considerable reactivity with HOI near neutral pH ($k_{app} = 9.8 \times 10^3$ and $6.3 \times 10^4 \text{ M}^{-1}\text{s}^{-1}$ at pH 7.1 and 8.0, respectively). The species-specific second order rate constants for the reactions of H_2O_2 with HOI, HO_2^- with HOI, and HO_2^- with OI^- were determined as $k_{H_2O_2+HOI} = 29 \pm 5.2 \text{ M}^{-1}\text{s}^{-1}$, $k_{HO_2^-+HOI} = (3.1 \pm 0.3) \times 10^8 \text{ M}^{-1}\text{s}^{-1}$, and $k_{HO_2^-+OI^-} = (6.4 \pm 1.4) \times 10^7 \text{ M}^{-1}\text{s}^{-1}$, respectively. The activation energy for the reaction between HOI and H_2O_2 was determined to be $E_a = 34 \text{ kJ mol}^{-1}$. The effect of buffer types (phosphate, acetate, and borate) and their concentrations was also investigated. Phosphate and acetate buffers significantly increased the rate of the H_2O_2 –HOI reaction at pH 7.3 and 4.7, respectively, whereas the effect of borate was moderate. It could be demonstrated, that the formation of iodophenols from phenol as a model for I-DBPs formation was significantly reduced by the addition of H_2O_2 to HOI- and phenol-containing solutions. During water treatment with the O_3/H_2O_2 process or peracetic acid in the presence of I^- , O_3 and peracetic acid will be consumed by a catalytic oxidation of I^- due to the fast reduction of HOI by H_2O_2 . The O_3 deposition on the ocean surface may also be influenced by the presence of H_2O_2 , which leads to a catalytic consumption of O_3 by I^- .

© 2020 The Authors. Published by Elsevier Ltd. This is an open access article under the CC BY license (<http://creativecommons.org/licenses/by/4.0/>).

1. Introduction

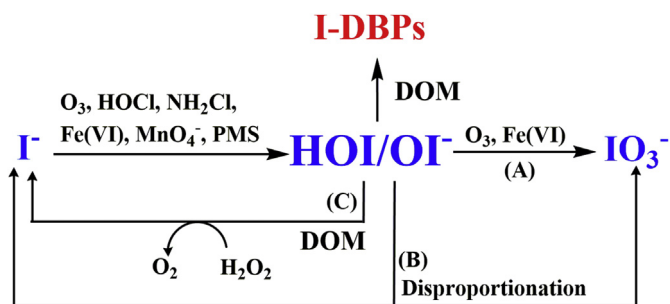
During oxidative water treatment at circumneutral pH, iodide (I^-) is rapidly oxidized to aqueous iodine, mainly hypoiodous acid (HOI), which has a high potential to produce iodinated disinfection byproducts (I-DBPs) by its reactions with dissolved organic matter moieties (Bichsel and von Gunten, 1999; Bichsel and von Gunten, 2000a; Criquet et al., 2012; Allard et al., 2015). As a consequence, I-DBPs have been widely detected in oxidatively treated iodide-

containing waters (Krasner et al., 2006; Wei et al., 2013; Gong and Zhang, 2015; Pan et al., 2016). The formation of I-DBPs is of concern in drinking water because they are more cytotoxic, genotoxic, and mutagenic than their chlorinated and brominated analogues (Plewa et al., 2004; Richardson et al., 2008; Yang et al., 2014; Dong et al., 2019). Moreover, iodinated trihalomethanes (I-THMs), especially iodoform, can lead to an undesired medicinal taste and odor in finished drinking waters (Hansson et al., 1987).

To minimize the formation of I-DBPs, several studies have investigated the reactions of HOI with (in)organic constituents and various oxidants during drinking water treatment. HOI can be transformed by three competing pathways (Scheme 1): (A) oxidation to iodate (IO_3^-), (B) disproportionation to I^- and IO_3^- , and (C) reduction to I^- by dissolved organic matter (DOM) or hydrogen peroxide (H_2O_2) (Nagy

* Corresponding author. School of Architecture, Civil and Environmental Engineering (ENAC), École Polytechnique Fédérale de Lausanne (EPFL), CH-1015, Lausanne, Switzerland.

E-mail address: vongunten@eawag.ch (U. von Gunten).



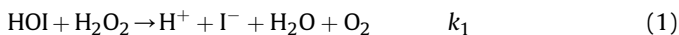
Scheme 1. Transformation pathways of I^- and HOI/OI^- during treatment of waters containing dissolved organic matter (DOM) with different oxidants.

et al., 1988; Bichsel and von Gunten, 1999; Bichsel and von Gunten, 2000a; Zhao et al., 2016; Li et al., 2017; Shin et al., 2018).

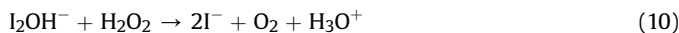
Iodate (IO_3^-) is nontoxic and thus the desired sink for iodine during oxidative water treatment (Bürgi et al., 2001), however, many oxidants (i.e., chlorine, chlorine dioxide, chloramine, permanganate, manganese dioxide) have relatively low reactivity with HOI, wherefore, IO_3^- formation is slow or absent (Bichsel and von Gunten, 2000a; Zhao et al., 2016). During chlorination of bromide-containing water, the oxidation of HOI to IO_3^- is significantly enhanced by HOBr ($k_{HOBr+OI^-} = 1.9 \times 10^6 \text{ M}^{-1}\text{s}^{-1}$), which is formed by the oxidation of bromide by chlorine (Criquet et al., 2012). However, at the same time, the formation of brominated I-DBPs is enhanced in the presence of bromide (Allard et al., 2015). Only ozone (O_3) and ferrate ($Fe(VI)$) show significant potential for a mitigation of I-DBPs by formation of IO_3^- through rapid oxidation of HOI (pH 7: $k_{appO_3+HOI/OI^-} = 3.7 \times 10^4 \text{ M}^{-1}\text{s}^{-1}$ and $k_{appFe(VI)+HOI/OI^-} = 1.5 \times 10^5 \text{ M}^{-1}\text{s}^{-1}$) (Bichsel and von Gunten, 1999; Shin et al., 2018). The formation of I-DBPs can also be minimized by reduction of HOI by reducing agents such as hydrogen peroxide (H_2O_2) (Shah et al., 2015a; Shin et al., 2018). H_2O_2 is widely used in oxidative water treatment, and intentionally added for some advanced oxidation processes (e.g., O_3/H_2O_2 or UV/H_2O_2). H_2O_2 is also present during various water treatment applications with peracids, such as peracetic acid (Shah et al., 2015a). Moreover, significant concentrations of H_2O_2 (20–30% of the consumed $Fe(VI)$) can be produced during treatment with $Fe(VI)$ by self-decay of $Fe(VI)$ (Lee et al., 2014).

During water treatment or in natural systems, HOI is the dominant species compared to molecular iodine (I_2) because the I^- concentration is typically very low (maximum $\sim 100 \mu\text{g/L}$ of I^- in surface water) and hence the equilibrium is on the side of HOI (Eq. (5) in Table 1) (Smedley, 2000; Moran et al., 2002; Richardson et al., 2008).

The reactions of iodine with H_2O_2 have been studied previously. Eq. (1) was proposed as a dominant reaction pathway in the $HOI-H_2O_2$ system (Bray and Liebhafsky, 1931). Eqs. (2)–(4) are based on the speciation of HOI/OI^- ($pK_{a1} = 10.4$) and H_2O_2/HO_2^- ($pK_{a2} = 11.8$).



The reported values of k_1 ($5-200 \text{ M}^{-1}\text{s}^{-1}$) (Bray and Liebhafsky, 1931; Furrow, 1987; Ishigure et al., 1986; Schmitz, 2010) and k_3 ($1.4 \times 10^7-6.0 \times 10^9 \text{ M}^{-1}\text{s}^{-1}$) (Liebhafsky, 1932; Ishigure et al., 1986; Shiraishi et al., 1992) vary over several orders of magnitude in literature (Table 2). This might be related to experimental differences. Previously, to determine the second order rate constants for the reaction of HOI with H_2O_2 , an indirect method was used, which measures the decrease of I_3^- in presence of excess I^- based on Eqs. (5) and (6) in Table 1. This approach can lead to different I_2 concentrations depending on the experimental conditions (e.g., pH, $[I_2]$, or $[I^-]_0$), wherefore, the reaction system may be ill-defined. Based on this approach, different pH-dependences of second order rate constants were found in several studies (e.g., $k \propto 1/[H^+]^2$) for the reaction of HOI with H_2O_2 . As a consequence, reactions in Eqs. (9) and (10) were introduced as a dominant reaction pathway in some previous studies (Shiraishi et al., 1992; Ball and Hnativ, 2001).



Overall, a lot of conflicting information for the kinetics of the reaction of HOI with H_2O_2 has been published, however, so far, no agreement has been reached, mainly due to the utilization of an indirect experimental approach.

In this study, second order rate constants for the reactions of HOI with H_2O_2 were directly determined by measuring the HOI decrease or I^- formation over a wide pH range from 4.0 to 12.0 using stopped-flow and batch-type experiments, excluding the formation and reactions of I_2 . This approach makes it possible to assess the importance of the reduction of HOI by H_2O_2 compared to its other reactions in water treatment and H_2O_2 -containing natural waters.

2. Materials and methods

2.1. Standards and reagents

All experiments were carried out with ultrapure water from a Milli-Q (Millipore) nanopure system. All chemicals and solvents were of the highest purity available and used as received without further purification (Supporting information, SI-Text 1). Hydrogen peroxide (H_2O_2) stock solutions were prepared by diluting a commercial solution of H_2O_2 (30 wt% in H_2O , Sigma) and standardized spectrophotometrically using the molar absorption coefficient of H_2O_2 ($\epsilon = 40 \text{ M}^{-1} \text{ cm}^{-1}$ at 240 nm (Bader et al., 1988)). Chlorine ($HOCl/OCl^-$) stock solutions were prepared by diluting a commercial sodium hypochlorite solution (10–15%, Sigma) and standardized spectrophotometrically using the molar absorption coefficient

Table 1
Reactions and equilibrium constants for iodine and hydrogen peroxide in aqueous solution.

Number	Reaction	K_{eq} or K_a	pK_a	reference
5	$I_2 + H_2O \rightleftharpoons HOI + I^- + H^+$	$5.44 \times 10^{-13} \text{ M}^2$		Burger and Liebhafsky (1973)
6	$I_2 + I^- \rightleftharpoons I_3^-$	725 M^{-1}		Burger and Liebhafsky (1973)
7	$HOI \rightleftharpoons H^+ + OI^-$	$4.0 \times 10^{-11} \text{ M}$	10.4	Bichsel and von Gunten (2000)
8	$H_2O_2 \rightleftharpoons H^+ + HO_2^-$	$2.5 \times 10^{-12} \text{ M}$	11.6	Staelin and Hoigné (1982)

Table 2Second order rate constants [$M^{-1}s^{-1}$] for reactions of H_2O_2/HO_2^- with HOI/OI^- , $HOBr/OBr^-$, and $HOCl/OCl^-$.

	$H_2O_2, M^{-1}s^{-1}$	Reference	$HO_2^-, M^{-1}s^{-1}$	Reference
HOI	29 ± 5.2 37 200 5 23	This study Liebhafsky (1932) Ishigure et al. (1986) Furrow (1987) Schmitz (2010)	$(3.1 \pm 0.3) \times 10^8$	This study
OI^-	6.0×10^9 1.4×10^7 6.6×10^7	Liebhafsky (1932) Ishigure et al. (1986) Shiraishi et al. (1992)	$(6.4 \pm 1.4) \times 10^7$	This study
HOBr	1.5×10^4	von Gunten and Oliveras (1997)	7.6×10^8	von Gunten and Oliveras (1997)
HOCl	–	–	4.4×10^7	Held et al. (1978)

of OCl^- (pH > 11, $\epsilon = 350 M^{-1} cm^{-1}$ at 292 nm (Kumar and Margerum, 1987)). Stock solutions of HOI (5–25 μM) were freshly prepared through oxidation of a slight excess of iodide (5.1–25.5 μM) by chlorine (5–25 μM) in pure water.

2.2. Kinetic experiments with stopped-flow

Kinetic studies for the reactions of HOI with H_2O_2 were performed under pseudo-first order conditions with H_2O_2 in molar excess over HOI with a Hi-Tech Scientific SF-61DX2 stopped-flow spectrometer (TgK Scientific, United Kingdom) in the pH range from 7.1 to 12 at 22 ± 2 °C. Initial concentrations of H_2O_2 were at least 4 times higher than HOI. A wide range (12 – 16'000 μM) of H_2O_2 solutions were prepared in different buffer solutions (Table S1, SI). HOI solutions at concentrations of 6 μM were in the same buffer solutions as the H_2O_2 solutions to avoid mixing problems. Buffered H_2O_2 and HOI solutions were then mixed in a 1:1 ratio to initiate the reaction and the formation of I^- was determined spectrophotometrically at 226 nm ($\epsilon_{226nm} = 1.36 \times 10^4 M^{-1} cm^{-1}$; the UV spectrum of I^- is shown in Fig. S1 (SI)). The UV absorption of I^- was not affected by the other reactants (i.e., H_2O_2 and HOI), because their molar absorption coefficients at 226 nm are much lower ($\epsilon < 80 M^{-1} cm^{-1}$) and their concentrations change proportionally with I^- . Therefore, the changes of the absorption at 226 nm are proportional to the relative changes of the I^- concentration, which can be used to calculate the apparent first order rate constant. The average I^- formation curves were calculated from at least eight replicate curves for each experimental condition. Pseudo-first order rate constants (k_{obs}) were then calculated by an exponential regression (with the software *Kinetic studio 2.x*, TgK Scientific) from the average I^- formation curves.

2.3. Kinetic experiments with the ABTS method in batch reactors

Lower second order rate constants for the reactions of HOI with H_2O_2 in the pH range 4–6.2 were determined by the ABTS method (Pinkernell et al., 2000; Shin et al., 2018). The kinetic experiments were conducted under pseudo-first order conditions with 1 μM (or 2 μM) HOI with a molar excess of H_2O_2 (20–200 μM) in the presence of 100 μM of $AgNO_3$. Ag^+ was added to quench I^- by forming AgI ($K_{so} = 8.5 \times 10^{-17}$) (Lide, 2006) and hence suppress the formation and the reactions of I_2 . This enabled us to determine the second order rate constants of the reaction of HOI with H_2O_2 at low and neutral pHs. The reaction was initiated by adding a small volume (≤ 1 mL) of a H_2O_2 stock solution (20 mM) under vigorous mixing to a buffered solution (100 mL) containing HOI. The reaction solutions were then quenched with an ABTS solution after certain reaction times to measure the residual HOI concentrations (Pinkernell et al., 2000).

2.4. Formation of iodophenols in HOI-, H_2O_2 -, and phenol-containing waters

Solutions (20 mL) containing phenol (10 μM), H_2O_2 (0–50 μM), and $AgNO_3$ (100 μM) were prepared in glass bottles and then reactions were initiated by adding 1 μM HOI at pH 7.0 (8 mM phosphate) and pH 9.0 (8 mM phosphate + 4 mM borate) under rapid mixing (10 s).

Iodo-phenols (2-iodo- and 4-iodo-phenols) were analyzed by HPLC (Dionex Ultimate 3000, USA) with UV detection at 231 nm. The separation was achieved by a Machery-Nagel C18 column using a mobile phase consisting of 70% 10 mM phosphoric acid and 30% methanol. The limit of quantification (LOQ) for both 2-iodophenol and 4-iodophenol was 0.05 μM .

2.5. Data analysis

The species-specific second order rate constants were determined from the pH-dependent apparent second order rate constants by using the software GraphPad Prism (www.graphpad.com). Model calculations to evaluate the influence of H_2O_2 during various oxidative water treatment in the presence of I^- were performed using Kintecus (Ianni, 2017).

3. Results and discussion

3.1. Determination of reaction order and second order rate constants

At pH 7 or higher, the reaction kinetics for the reactions of HOI with H_2O_2 followed a second-order rate law under our experimental conditions (Table S1, SI). During the reaction of HOI with excess H_2O_2 , the evolution of I^- was exponential, indicating that the reaction is pseudo first-order with respect to the H_2O_2 concentration (Fig. S2, SI). k_{obs} was calculated by an exponential regression (with the software *Kinetic studio 2.x*) from the I^- formation curves (Fig. S2, SI) and alternatively was also obtained from the slopes of the linear plots of the logarithmic relative residual concentration of HOI versus time (Fig. S3, SI). The relative residual concentration of HOI was calculated from the formation of I^- (Eq. (11)).

$$-\ln \frac{[HOI]_0 - [I^-]}{[HOI]_0} = k_{obs} \times time \quad (11)$$

The obtained k_{obs} values for the two methods were within 7.6% (Figures S2 and S3, SI). Fig. S4 (SI) shows the linearity of k_{obs} as a function of the H_2O_2 concentration ($R^2 \geq 0.999$) at pHs 8 and 9. The inset shows that the $\log(k_{obs})$ versus $\log([H_2O_2]_0)$ plot has a slope of 1 confirming a reaction order of one with respect to H_2O_2 . Based on this, apparent second-order rate constants (k_{app}) were determined by dividing k_{obs} by the corresponding initial H_2O_2

concentrations (Eq. (12)). The calculated k_{app} values were $6.3 \times 10^4 \text{ M}^{-1}\text{s}^{-1}$ at pH 8.0 and $3.7 \times 10^5 \text{ M}^{-1}\text{s}^{-1}$ at pH 9.0 (Table S1 (SI) and Fig. 1 and Fig. S4 (SI)).

$$k_{app} = k_{obs}/[\text{H}_2\text{O}_2]_0 \quad (12)$$

For $\text{pH} < 7.0$, the kinetics for the reaction of HOI with H_2O_2 did not follow pseudo-first order ($1\text{--}3 \mu\text{M}$ HOI in excess of H_2O_2). This is illustrated as an example in Fig. S5 (SI), for pH 6 (HOI ($3 \mu\text{M}$) with excess H_2O_2 ($1, 2, \text{ and } 4 \text{ mM}$)). This is due to the presence of I_2 leading to several competitive reactions, which may have caused the wide range of reported second order rate constants for the reaction of HOI with H_2O_2 in the literature (Table 2). Since I^- is produced during the reaction of HOI with H_2O_2 , the I_2 concentration increases with increasing formation of I^- in the course of the reaction, especially at low pH (Eq. (5), Table 1). Fig. S6 (SI) shows the speciation of $\text{I}_2/\text{HOI}/\text{OI}^-$ depending on I^- concentrations (0.1 and $2.0 \mu\text{M}$) as a function of pH. HOI is the major species in the neutral pH ($6\text{--}9$) in the presence of low concentration of I^- (e.g., $0.1 \mu\text{M}$). Meanwhile, I_2 is the major species in presence of a high concentration of I^- (e.g., $2.0 \mu\text{M}$) for a $\text{pH} < 6.5$.

To exclude the effect of I^- , $100 \mu\text{M}$ Ag^+ was added before initiating the reactions at $\text{pH} < 7.0$, to avoid the formation of I_2 (see above). Under these conditions, the decrease of HOI ($[\text{HOI}]_0 = 1$ or $2 \mu\text{M}$) in the presence of excess H_2O_2 ($20\text{--}200 \mu\text{M}$) showed pseudo-first order kinetics (Fig. S7, SI). Second order rate constants (k_{app}) were determined by Eq. (13), yielding $34 \pm 1 \text{ M}^{-1}\text{s}^{-1}$, $84 \pm 8 \text{ M}^{-1}\text{s}^{-1}$, and $940 \pm 60 \text{ M}^{-1}\text{s}^{-1}$ at pHs 4, 5, and 6, respectively.

$$-\ln \frac{[\text{HOI}]}{[\text{HOI}]_0} = k_{app} \times [\text{H}_2\text{O}_2]_0 \times \text{time} \quad (13)$$

3.2. pH dependence of the second order rate constant for the reaction between hypiodous acid and hydrogen peroxide

Table S1 (SI) compiles the observed pH-dependent first-order rate constants (k_{obs}) and apparent second-order rate constants (k_{app}) for the reactions of HOI with H_2O_2 . The k_{app} are also plotted in Fig. 1 for the pH range 4–12. In general, the k_{app} values increase with increasing pH, which can be explained by the speciation of HOI and H_2O_2 ($\text{p}K_{a1}(\text{HOI}/\text{OI}^-) = 10.4$ and $\text{p}K_{a2}(\text{H}_2\text{O}_2/\text{HO}_2^-) = 11.8$). Acid-base equilibria are considered to be faster than the redox reactions. From a kinetic point of view, the reactions in Eqs. (2) and (3) cannot be distinguished because they have the same pH dependence. Rather than considering the two reactions in parallel, it is assumed that only one of the two pathways is important. In the HOI– H_2O_2 systems, HOI is more electrophilic than OI^- , and HO_2^- is stronger nucleophile than H_2O_2 . Therefore, the reaction of HOI with HO_2^- (Eq. (2)) is considered the major pathway for the reaction of HOI with H_2O_2 . The same mechanistic interpretations for the HOCl– H_2O_2 and HOBr– H_2O_2 systems are discussed in the literature (Held et al., 1978; von Gunten and Oliveras, 1997). Meanwhile, at low or high pH, the reactions of HOI with H_2O_2 or OI^- with HO_2^- , respectively, can also occur. Therefore, Eqs. (1), (2) and (4) should be considered to determine the species-specific second order rate constants.

The pH-dependent variation in k_{app} could be quantitatively modeled by Eq. (14), considering the species-specific reactions between HOI/ OI^- and $\text{H}_2\text{O}_2/\text{HO}_2^-$.

$$k_{app} = k_1 \alpha_{\text{HOI}} \beta_{\text{H}_2\text{O}_2} + k_2 \alpha_{\text{HOI}} \beta_{\text{HO}_2^-} + k_4 \alpha_{\text{OI}^-} \beta_{\text{HO}_2^-} \quad (14)$$

where k_1 , k_2 , and k_4 are the species-specific second order rate constants in Eqs. (1), (2) and (4), respectively. α_{HOI} , α_{OI^-} , $\beta_{\text{H}_2\text{O}_2}$, and

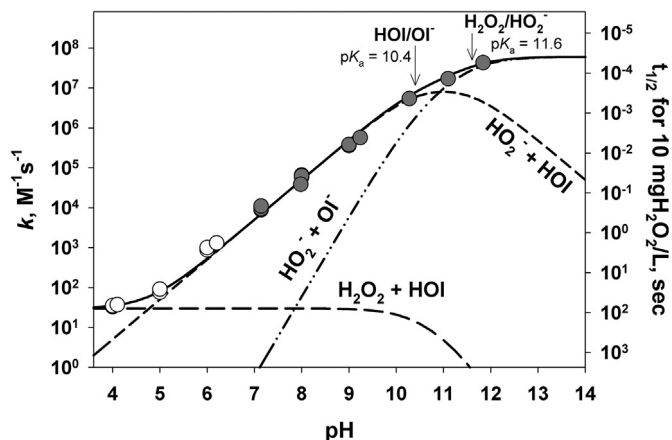


Fig. 1. Apparent second-order rate constants (k_{app} , left-axis) for the reaction of HOI with H_2O_2 and half-lives for the HOI abatement in presence of 10 mg L^{-1} H_2O_2 ($t_{1/2}$, right-axis) as a function of pH (4.0–11.8). The closed circles represent the k_{app} values determined with stopped-flow measurements and the open circles represent the k_{app} values determined by the ABTS method in a batch system in the presence of AgNO_3 . The solid line represents the calculated k_{app} for the reaction of HOI with H_2O_2 according to Eq. (14) in the text. The other lines represent the calculated contributions of the reactions of HOI with HO_2^- (dashed), OI^- with HO_2^- (dotted-dashed), and HOI with H_2O_2 (long dashed) to the overall reaction as a function of the pH.

$\beta_{\text{HO}_2^-}$ represent the fractions of HOI, OI^- , H_2O_2 , and HO_2^- , respectively, which, at a given pH can be expressed as $\alpha_{\text{HOI}} = [\text{H}^+]/([\text{H}^+] + K_{a,\text{HOI}})$, $\alpha_{\text{OI}^-} = K_{a,\text{HOI}}/([\text{H}^+] + K_{a,\text{HOI}})$, $\beta_{\text{H}_2\text{O}_2} = [\text{H}^+]/([\text{H}^+] + K_{a,\text{H}_2\text{O}_2})$, and $\beta_{\text{HO}_2^-} = K_{a,\text{H}_2\text{O}_2}/([\text{H}^+] + K_{a,\text{H}_2\text{O}_2})$, with K_a being the corresponding acid-base equilibrium constants (see Table 1). The species-specific second order rate constants were calculated from least squares nonlinear regressions of the experimental k_{app} data (Table S1, SI) using the GraphPad Prism (www.graphpad.com). The model could fit the experimental k_{app} well ($R^2 > 0.92$). The species-specific second order rate constants were determined to be $k_1(\text{HOI} + \text{H}_2\text{O}_2) = 29 \pm 5.2 \text{ M}^{-1}\text{s}^{-1}$, $k_2(\text{HOI} + \text{HO}_2^-) = (3.1 \pm 0.3) \times 10^8 \text{ M}^{-1}\text{s}^{-1}$, $k_4(\text{OI}^- + \text{HO}_2^-) = (6.4 \pm 1.4) \times 10^7 \text{ M}^{-1}\text{s}^{-1}$ (Table 2). The error ranges for k_1 , k_2 , and k_4 are due to experimental variabilities and also due to the types and concentrations of the buffers.

The second order rate constants for the reactions of HOI with H_2O_2 can be applied to calculate the half-life of HOI in H_2O_2 containing water treatment. The calculations of the half-life of HOI are shown in Fig. 1 for 10 mg L^{-1} H_2O_2 , which is an intermediate-high range dose applied to advanced oxidation processes (AOPs) (Stefan, 2017). Half-lives for the HOI abatement in the presence of 10 mg/L of H_2O_2 are 4.4, 0.47, and 0.047 s at pH 6, 7, and 8, respectively.

3.3. Effect of the buffer type and concentrations on the kinetics of the reactions of HOI with H_2O_2

Previous studies have shown that buffer type and concentrations can influence the reactivity of HOI with oxidants (i.e., ferrate(VI) or permanganate(VII)) (Wang et al., 2018; Zhao et al., 2016) or phenols (Zhao et al., 2017) and the disproportionation of HOI (Bichsel and von Gunten, 2000b). The effects of different buffers (phosphate, borate, and acetate) at different pHs (pH 7.3, 9.0, and 4.7) on the reduction of HOI by H_2O_2 were investigated (Table S2 and Figs. S8–S10 (SI)). During the reaction of HOI ($3 \mu\text{M}$) with H_2O_2 (4 mM at pH 7.3, $40 \mu\text{M}$ at pH 9.0), an exponential increase of I^- was monitored by stopped-flow in the presence of various concentrations of phosphate ($\text{p}K_a = 7.2$ for H_2PO_4^- (Goldberg et al., 2002)) or borate buffer ($\text{p}K_a = 9.2$ (Goldberg et al., 2002)) (Figs. S8 and S9 (SI)). At pH 4.7, the kinetics of the reactions of HOI with H_2O_2

follow pseudo first order in the presence of 100 μM of Ag^+ with various concentrations of acetate ($\text{p}K_a = 4.76$ (Goldberg et al., 2002)) (Fig. S10, SI). The rates of I^- formation and hence the HOI consumption increased with increasing phosphate, borate, and acetate concentrations. This indicates that the selected buffers enhance the reaction of HOI with H_2O_2 . Among the selected buffers, phosphate shows the most significant enhancement of the reactivity, especially at pH 7.3 (Fig. S11, SI). At pH 7.3, k_{app} in presence of 1.25 mM phosphate buffer was $7.6 \times 10^3 \text{ M}^{-1}\text{s}^{-1}$, which increased up to a factor of 4.3 for 25 mM phosphate ($k_{app} = 3.3 \times 10^4 \text{ M}^{-1}\text{s}^{-1}$). However, the effect of phosphate was less pronounced at pH 9.0. The reaction in presence of 50 mM phosphate was 1.6 times faster than without phosphate. Meanwhile, acetate enhanced the apparent second order rate constant from $52 \text{ M}^{-1}\text{s}^{-1}$ (1 mM acetate) to $140 \text{ M}^{-1}\text{s}^{-1}$ (25 mM acetate) at pH 4.7. Borate showed lower effects on the apparent second order rate constants, which ranged from $2.5 \times 10^5 \text{ M}^{-1}\text{s}^{-1}$ (0.5 mM borate) to $5.4 \times 10^5 \text{ M}^{-1}\text{s}^{-1}$ (25 mM borate). The rate constants at zero buffer concentrations were also estimated by a linear regression based on Fig. S11 (SI). The y-axis intercept indicates each second order rate constant at zero buffer concentration ($40.7 \text{ M}^{-1}\text{s}^{-1}$ at pH 4.7, $5.6 \times 10^3 \text{ M}^{-1}\text{s}^{-1}$ at pH 7.3, and $2.4 \times 10^5 \text{ M}^{-1}\text{s}^{-1}$ at pH 9.0). These second order rate constants are compared in Fig. S12 (SI) with the determined k_{app} (Fig. 1 and Table S1, SI) which were used for determining the species-specific rate constants. The measured k_{app} values at 3–6 mM acetate buffer (pH 4–5), at 5–10 mM phosphate buffer (pH 6–8), and at 5–10 mM borate buffer (pH ≥ 9) might be overestimated at most 2.4-, 3.2-, 1.7-fold, respectively, which is in the range of variations of experimental second order rate constants.

3.4. Temperature effect on the kinetics of the reduction of HOI by H_2O_2

The effect of temperature on the kinetics of the reaction of HOI with H_2O_2 was studied at 10.0–23.2 $^\circ\text{C}$ at pH 9.0 (5 mM phosphate + 5 mM borate buffer) (Fig. S13, SI). An Arrhenius plot shows good linearity ($R^2 = 0.98$), between the logarithm of the apparent second order rate constants and the reciprocal of the absolute temperature (T) (Eq. (15)).

$$\ln k_{app} = \frac{-E_a}{R} \times \frac{1}{T} + \ln A \quad (15)$$

where A is a frequency factor, E_a is the apparent activation energy (J mol^{-1}), R ($8.314 \text{ J mol}^{-1}\text{K}^{-1}$) is the ideal gas constant, and T is absolute temperature (K). Based on Eq. (15) (Fig. S13, SI) an E_a of 34 kJ mol^{-1} can be obtained. This is significantly lower than the E_a value of 125 kJ mol^{-1} reported for the reaction of I_2 with H_2O_2 (Ball and Hnatiw, 2001).

3.5. Formation of iodophenols in HOI-, H_2O_2 -, and phenol-containing waters

To evaluate the effect of H_2O_2 on the formation of I-DBPs during oxidation processes, in which H_2O_2 is present (e.g., $\text{O}_3/\text{H}_2\text{O}_2$, UV/ H_2O_2 , ferrate(VI), peracetic acid treatment), phenol was added as a simplified surrogate for DOM and the formed iodophenols were quantified as a proxy for the extent of I-DBPs formation. The second order rate constant of the reaction of HOI with phenol is similar to the reaction of HOI with H_2O_2 at pH 7 (i.e., $k_{\text{HOI}+\text{phenol}} = 2.6 \times 10^3 \text{ M}^{-1}\text{s}^{-1}$ (Bichsel and von Gunten, 2000a) and $k_{\text{HOI}+\text{H}_2\text{O}_2} = 4.9 \times 10^3 \text{ M}^{-1}\text{s}^{-1}$ at pH 7.0 (this study)), 2-iodophenol and 4-iodophenol were detected during the reaction of HOI (1 μM) with phenol (10 μM) in the presence of varying concentrations of H_2O_2 (0–50 μM) at pH 7.0 (8 mM

phosphate) and pH 9.0 (8 mM phosphate + 4 mM borate). Ag^+ was added to exclude the formation and reactions of I_2 . A HOI concentration of 1 μM was chosen to simulate an elevated I^- level (130 $\mu\text{g/L}$) and the concentration of phenol was 10 times that of HOI. 10 μM ($\sim 0.94 \text{ mg/L}$) of phenol would correspond to a source water containing about 5 mgC/L DOC with a typical phenol content of around 20% (Önnby et al., 2018).

H_2O_2 is generally applied as 2–15 mg/L in advanced oxidation processes (Stefan, 2017). Nevertheless, relatively low concentrations of H_2O_2 ($\leq 2 \text{ mg/L}$) were applied here to evaluate the trend of iodophenol formation.

Fig. 2 shows that HOI was fully transformed to iodophenols during the reaction of HOI with phenol in the absence of H_2O_2 at pHs 7.0 and 9.0. As expected, the formation of iodophenols decreased with increasing H_2O_2 doses and at the maximum H_2O_2 concentration of about 1.7 mg/L (50 μM) only low concentrations of iodophenols ($< 0.1 \mu\text{M}$) were detected due to the reduction of HOI by H_2O_2 to I^- . Even with these relatively low H_2O_2 doses, a large effect on the minimization of the formation of iodophenols was observed. Similar levels of iodophenol formation were observed at both pH 7.0 and 9.0. This is because k_{app} of the reaction of HOI with phenol and the reaction of HOI with H_2O_2 exhibit a similar pH dependency, with generally increasing apparent second order rate constants with increasing pH (Bichsel and von Gunten, 2000a; Zhao et al., 2017). The modeling results based on the reaction in Table S3 (SI) for the iodophenol formation were slightly higher than the experimental data by a factor of 1.05–1.15 at pH 7.0 and 1.1–1.3 at pH 9.0 (Fig. 2a and b, dashed lines with circles). This can be considered as a good agreement given the uncertainty in the values of the second order rate constants for the involved reactions.

3.6. Comparison of the reactivities of H_2O_2 with HOI, HOCl, and HOBr

Fig. 3 and Table 2 show a comparison of the apparent and species-specific second order rate constants for the reactions of H_2O_2 with HOI, HOBr, and HOCl, respectively. The species-specific second order rate constants for the reaction of HO_2^- with HOX, decrease in the order HOBr ($7.6 \times 10^8 \text{ M}^{-1}\text{s}^{-1}$) > HOI ($3.1 \times 10^8 \text{ M}^{-1}\text{s}^{-1}$) > HOCl ($4.4 \times 10^7 \text{ M}^{-1}\text{s}^{-1}$). This sequence has also been observed for electrophilic aromatic substitution reactions of HOX with phenols (Heeb et al., 2014). Based on the standard reduction potentials it would be expected that HOCl has the highest reactivity. However, since the reaction potentially involves a X^+ transfer to HO_2^- (Heeb et al., 2014), the partial positive charge on X in HOX is also important. The electronegativity of the halogens decreases in the order $\text{Cl} > \text{Br} > \text{I}$, wherefore, the partial positive charge increases in the order $\text{Cl} < \text{Br} < \text{I}$. Based on this consideration, HOI should have the highest reactivity to form the H–O–O–X intermediate. This species decomposes under the formation of X^- and singlet oxygen. This reaction step is favored again by the more electrophilic halogen. Overall, the combination of these factors then leads to the observed sequence for the species-specific second order rate constants for the reactions of HOX with H_2O_2 . The only exception was observed from the reaction of HO_2^- with OI^- . In the literature, the reaction of HO_2^- with hypohalite ions (OBr^- and OCl^-) were not considered because of the strongly reduced partial positive charge on Br and Cl for the hypohalite ions. Meanwhile, the reaction of HO_2^- with OI^- was the major reaction at high pH (> 11.0). This may be due to the lower electronegativity of I compared to Br or Cl, which means that there is still a significant partial positive charge on I in OI^- .

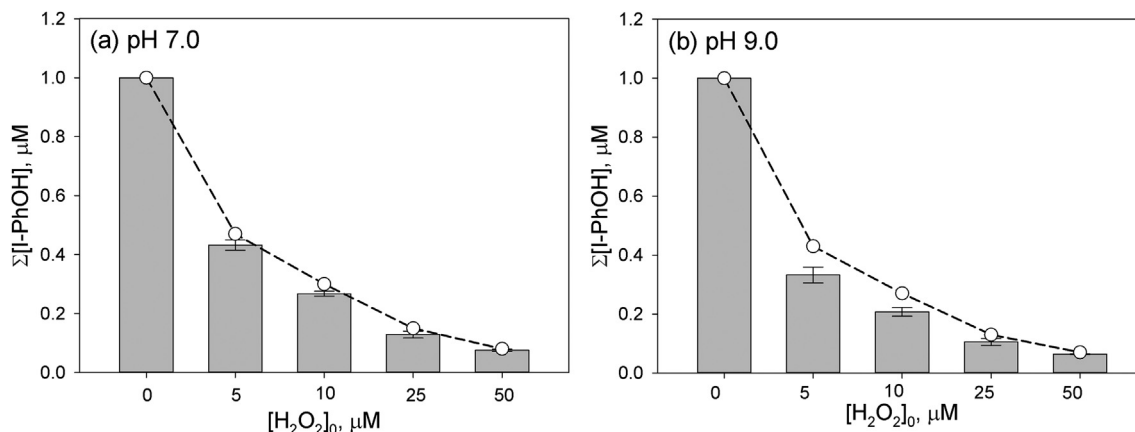


Fig. 2. Measured and modeled formation of iodo-phenols during the reaction of HOI with phenol as a function of increasing H_2O_2 concentrations (0, 5, 10, 25, and 50 μM) for (a) pH 7.0 (8 mM phosphate) and (b) pH 9.0 (8 mM phosphate + 4 mM borate). Experimental conditions: $[\text{phenol}]_0 = 10 \mu\text{M}$, $[\text{HOI}]_0 = 1 \mu\text{M}$, and $[\text{AgNO}_3]_0 = 100 \mu\text{M}$. Each bar represents the mean value, and the error bars represent the range of values from duplicate experiments. Dashed lines with circles represent the model calculation by Kintecus (Ianni, 2017). The model calculations are based on the reactions in Table S3 (SI).

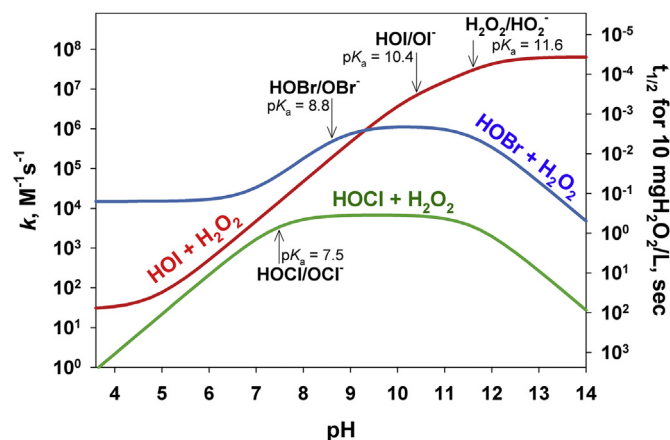


Fig. 3. Comparison of the pH-dependent apparent second-order rate constants for the reactions of H_2O_2 with HOI, HOBr, or HOCl. The rate constants for the reaction of H_2O_2 with HOCl were obtained from Held et al. (1978), and with HOBr from von Gunten and Oliveras (1997).

3.7. Implications for water treatment and natural systems

3.7.1. Water treatment

The formation of I-DBPs during drinking water disinfection has become an emerging concern. Their formation is initiated by the relatively easy oxidation of I^- to HOI by chemical oxidants during water treatment. However, most oxidants with the exception of O_3 and Fe(VI) have low reactivity with HOI, which leads to the formation of I-DBPs by the reaction of HOI with DOM. In certain processes, in which H_2O_2 is present together with a primary oxidant, the reduction of HOI to I^- by H_2O_2 needs to be considered due to the significant reactivity of the two compounds.

A recent study showed a constant I^- concentration during UV/ H_2O_2 treatment in the presence of 130 $\mu\text{g/L}$ of I^- , 10 mg/L of H_2O_2 , and 3.5 mg/L DOC at pH 7.0 (Zhang et al., 2018). In fact, in the UV/ H_2O_2 process, I^- is oxidized to HOI through the formation of radical species (i.e., I^\bullet , I_2^\bullet) by the rapid reaction with OH radical ($k \sim 10^{10} \text{ M}^{-1}\text{s}^{-1}$) (Elliot, 1992; Ellison et al., 1972; Nagarajan and Fessenden, 1985). However, the formed HOI will be quickly reduced to I^- by H_2O_2 . As already mentioned above, half-lives for the HOI abatement in the presence of 10 mg/L of H_2O_2 at neutral pH were low, namely 0.5 and 0.05 s at pH 7 and 8, respectively. Thus,

UV/ H_2O_2 pre-oxidation followed by chlorination or chloramination still has a risk of I-DBP formation due to the remaining I^- .

In the $\text{O}_3/\text{H}_2\text{O}_2$ process, I^- is quickly oxidized to HOI ($k_{\text{O}_3+\text{I}^-} = 2.0 \times 10^9 \text{ M}^{-1}\text{s}^{-1}$). The resulting hypiodous acid (HOI/OI $^-$) has two competing reaction pathways: (1) reduction to I^- by H_2O_2 ($k_{\text{HO}_2+\text{HOI}} = 3.1 \times 10^8 \text{ M}^{-1}\text{s}^{-1}$) and (2) oxidation to IO $_3^-$ through IO $_2^-$ by O_3 ($k_{\text{O}_3+\text{HOI}} = 3.6 \times 10^4 \text{ M}^{-1}\text{s}^{-1}$ and $k_{\text{O}_3+\text{OI}^-} = 1.6 \times 10^6 \text{ M}^{-1}\text{s}^{-1}$). Reduction of HOI by H_2O_2 could lead to the loss of oxidation capacity of O_3 by a catalytic cycle of oxidation of I^- by O_3 and reduction of HOI by H_2O_2 back to I^- . A kinetic simulation was used to calculate the relative contributions of various reactions to the O_3 consumption, i.e., catalytic oxidation of I^- , reaction with H_2O_2 , and further oxidation of HOI to IO $_3^-$. For simplicity, the formation and reactions of $\bullet\text{OH}$ were not considered in these model calculations. For the selected conditions of the $\text{O}_3/\text{H}_2\text{O}_2$ process, 56–66% of O_3 (i.e., 11.7–13.7 μM) was consumed by the catalytic oxidation of I^- (Fig. S14, SI), rather than for the formation of $\bullet\text{OH}$ via its reaction with H_2O_2 ($k_{\text{O}_3+\text{HO}_2^-} = 9.6 \times 10^6 \text{ M}^{-1}\text{s}^{-1}$) for an elevated level of I^- (e.g., 1 μM (~130 $\mu\text{g/L}$), $[\text{O}_3] = 1 \text{ mg/L}$ (20.8 μM) and $[\text{H}_2\text{O}_2] = (4\text{--}10 \text{ mg/L})$) at pH 8.0. IO $_3^-$ was the dominant iodine species only during ozonation with a low concentration of H_2O_2 ($[\text{H}_2\text{O}_2] \leq 2 \text{ mg/L}$) due to the fast reactions of O_3 with I^- and with HOI forming IO $_3^-$. However, significant concentrations of I^- could remain after complete consumption of O_3 in the presence of relatively high H_2O_2 ($[\text{H}_2\text{O}_2] > 2 \text{ mg/L}$). Such conditions are typically applied for bromate control during the $\text{O}_3/\text{H}_2\text{O}_2$ process (Pinkernell and von Gunten, 2001; Soltermann et al., 2017; von Gunten and Oliveras, 1997; von Gunten and Oliveras, 1998; von Sonntag and von Gunten, 2012). During post-disinfection with chlorine or chloramine, iodide can then be a precursor to I-DBPs. Therefore, if both I^- and Br^- are present in a source water, appropriate H_2O_2 doses should be applied during ozonation to minimize the formation of both I-DBPs and BrO_3^- .

Peracetic acid (PAA) is a disinfectant considered for use in ballast water and wastewater treatment (Luukkonen and Pehkonen, 2017; Shah et al., 2015a,b; Werschkun et al., 2014). H_2O_2 is always present in peracetic acid (PAA) solutions because PAA is synthesized by the reaction of acetic acid with H_2O_2 . To evaluate the role of H_2O_2 during the treatment of I^- and Br^- by PAA in an ocean-type water, a kinetic simulation was performed. Fig. S15 (SI) shows the evolutions of HOI, HOBr, H_2O_2 , and PAA during treatment of 0.5 μM I^- and 460 μM Br^- by 2.15 mM PAA in the presence of 0.65 mM H_2O_2 at pH 8.0. In this system, I^- and Br^- are oxidized to HOI and HOBr by

PAA ($k_{PAA+I^-} = 4.2 \times 10^2 \text{ M}^{-1}\text{s}^{-1}$, $k_{PAA+Br^-} = 0.24 \text{ M}^{-1}\text{s}^{-1}$) (Awad et al., 2003; Shah et al., 2015a), however, as soon as HOI or HOBr are produced, they are reduced by H_2O_2 to I^- or Br^- . These reactions continued until most of the H_2O_2 was consumed, and at the same time, PAA decreased to a similar extent as H_2O_2 . For the selected conditions (Fig. S15, SI) H_2O_2 was almost completely consumed at 20 min and I^- was rapidly oxidized to HOI whereas Br^- was slowly oxidized to HOBr by PAA. During PAA treatment, H_2O_2 can be a barrier for the formation I-DBPs or Br-DBPs by minimizing the lifetime of the hypohalous acids HOI and HOBr. However, it can also lead to a rapid consumption of PAA by an iodide-catalyzed reaction. This catalyzed reaction was also reported in a previous study (Shah et al., 2015a).

H_2O_2 is one of the major products during the self-decay of Fe(VI) (Lee et al., 2014). The yield of H_2O_2 ($\Delta[\text{H}_2\text{O}_2]/\Delta[\text{Fe(VI)}]$) was ~ 0.2 during the reaction of Fe(VI) with I^- or HOI (Shin et al., 2018). To assess the influence of H_2O_2 formation on the fate of iodine, a kinetic simulation was performed for treatment of I^- by Fe(VI). To better understand the effect of H_2O_2 , the following simplified boundary conditions were assumed: H_2O_2 was not produced during the Fe(VI) reactions but was initially present as 30% of Fe(VI). Fig. S16 (SI) shows the modeling results for the evolution of HOI, IO_3^- , H_2O_2 , and Fe(VI) during the treatment of $1 \mu\text{M}$ of I^- by $17.9 \mu\text{M}$ Fe(VI) (1 mgFe/L) in the presence of $5.4 \mu\text{M}$ H_2O_2 at pHs 7.0–9.0. At pH 7.0, 99% of I^- was oxidized to IO_3^- within 11 s by Fe(VI) without interference of H_2O_2 . With increasing pH from 7.0 to 9.0, the oxidation rate of I^- to IO_3^- decreased. This is because the rate of Fe(VI) reaction with HOI and I^- decreases with increasing pH (i.e., $k_{\text{Fe(VI)+HOI}} = 1.8 \times 10^5 \text{ M}^{-1}\text{s}^{-1}$ at pH 7.0 and $4.7 \times 10^3 \text{ M}^{-1}\text{s}^{-1}$ at pH 9.0) while the rate of HOI reduction by H_2O_2 to I^- increases. Overall an increase in pH led to an increase in the consumption of H_2O_2 and Fe(VI). At pH 7.0, only $3 \mu\text{M}$ of Fe(VI) was consumed to completely oxidize $1 \mu\text{M}$ I^- to IO_3^- without consumption of H_2O_2 , while, at pH 9.0, $8.4 \mu\text{M}$ of Fe(VI) was consumed with a H_2O_2 consumption of $5.6 \mu\text{M}$ for a full oxidation of I^- to IO_3^- .

3.7.2. Natural systems

O_3 deposition to the seawater surface is a significant mechanism for the loss of atmospheric O_3 , accounting for a loss of 600–1000 Tg $\text{O}_3 \text{ yr}^{-1}$ (Ganzeveld et al., 2009). Aqueous inorganic iodine (i.e., I^- , HOI) at the sea surface microlayer is one of the major contributors to the oceanic deposition of O_3 . This is based on the fast reaction between O_3 (gas) and I^- , which forms HOI in the aqueous phase and iodine oxide in the gaseous phase while O_3 is reduced to O_2 (Carpenter et al., 2013; Chang et al., 2004; Sarwar et al., 2015; Simpson et al., 2015). During this reaction, O_3 deposition might be significantly enhanced by H_2O_2 due to its high reactivity with HOI to form I^- . The concentration of H_2O_2 at the sea surface varies from 10 to $>500 \text{ nM}$ (Moore et al., 1993; Price et al., 1998; Zika et al., 1985). The gas-phase flux of O_3 into the boundary layer can be determined by the product of the O_3 deposition velocity (v_D) and the O_3 concentration ($[\text{O}_3(\text{gas})]$). The O_3 deposition velocity (v_D) over seawater is highly variable ($0.01\text{--}0.27 \text{ cm s}^{-1}$) (Ganzeveld et al., 2009; Helmig et al., 2012), depending on several factors in the seawater (i.e., water quality) and the atmosphere (e.g., wind).

A simplified isolated kinetic modeling was performed to assess the impact of the seawater concentrations of H_2O_2 on the O_3 deposition to the sea surface microlayer in the presence of I^- and Br^- (Fig. S17, SI). Since the source of O_3 is the atmosphere and the source of I^- , Br^- , and H_2O_2 is the ocean, it was assumed that the concentrations of each compound are in steady state. A steady-state concentration of HOI was applied instead of I^- since I^- is easily oxidized to HOI. Currently, HOI concentrations in the seawater are unknown due to the lack of analytical techniques with sufficient accuracy and sensitivity (Carpenter et al., 2013).

Considering the reported total inorganic iodine concentrations (e.g., I^- and IO_3^-) of 500 nM in seawater (Chance et al., 2014), the $[\text{HOI}]_{\text{ss}}$ was varied between 25–500 nM. With increasing $[\text{HOI}]_{\text{ss}}$, O_3 deposition increases (SI-Text-3 and Fig. S17 (SI)). In a next step, the $[\text{HOI}]_{\text{ss}}$ was fixed at an intermediate concentration of 100 nM and the steady-state concentrations of the other reactive species were assumed as follows: $[\text{O}_3]_{\text{ss}} = 1 \text{ nM}$, $[\text{Br}^-]_{\text{ss}} = 500 \mu\text{M}$, and variable $[\text{H}_2\text{O}_2]_{\text{ss}} = 0, 10, 25, 100, 250, 500 \text{ nM}$. Virtual reaction products as tracers (i.e., P1, P2, ...P7 in Table S4, SI) were quantified by Kintecus modeling to obtain the relative contributions of the various reactions to O_3 consumption (reactions 1 – 7 in Table S4, SI): (1) Oxidation of I^- was obtained from P3, (2) Oxidation of Br^- was obtained from P7, and (3) Oxidation of HOI to IO_3^- was determined by the summation of P4, P5, and P6. The reaction system reached steady-state within a few seconds, however, one year of modeling time was applied to obtain the total yearly O_3 deposition.

As the H_2O_2 concentration is increasing, the O_3 consumption for the oxidation of I^- becomes increasingly important compared to the reaction with bromide, which dominates at low H_2O_2 concentrations (Fig. S18a, SI). The contribution of the catalytic oxidation of I^- for the O_3 consumptions increased from 36% to 97% for an increase of H_2O_2 from 10 nM to 500 nM (Fig. S18a, SI). For all selected H_2O_2 concentrations, the consumption of O_3 by the oxidation of HOI to IO_3^- was insignificant ($<10\%$) compared to the O_3 consumption for the oxidation of I^- or Br^- .

In this kinetic modeling, the concentration of I^- reached steady-state within a few seconds. Fig. S18b (SI) shows that the resulting steady-state concentration of I^- ($[\text{I}^-]_{\text{ss}}$) and the total O_3 consumptions over 1 year depend on the initial $[\text{H}_2\text{O}_2]_{\text{ss}}$. According to kinetic modeling results, the $[\text{I}^-]_{\text{ss}}$ increased linearly with increasing H_2O_2 concentrations (0–500 nM). As a consequence, the total O_3 deposition rate increased proportionally (2.8–82.1 mM per year). If these results are combined with variable $[\text{HOI}]_{\text{ss}}$, the total O_3 deposition ranges from 3.6 mM (25 nM HOI/25 nM H_2O_2) to 400 mM (500 nM HOI/500 nM H_2O_2) per year.

Accounting for the area of the sea surface microlayer ($3.5 \times 10^8 \text{ km}^2$) (Costello et al., 2010) and setting the depth of the boundary layer to 100 μm , an O_3 deposition rate of 6.2–400 Tg/year can be calculated depending on the HOI (25–500 nM) and the H_2O_2 concentrations (0–500 nM). Depending on the boundary conditions, this deposition rate is about two orders of magnitude lower or in the same range as current estimates (see above). Therefore, our simplified estimate shows that H_2O_2 may have a high potential to increase the O_3 deposition by the catalytic oxidation of I^- at the sea surface, which might warrant an inclusion of these reactions to calculate O_3 deposition in future modeling efforts. The reduction of HOI by H_2O_2 can also occur in atmospheric waters, which may lead to a reduction of the O_3 levels in the troposphere (Pillar et al., 2013).

4. Conclusions

Apparent and species-specific second order rate constants for the reactions of hydrogen peroxide with hypiodous acid were determined and the main conclusions are as follows:

- The reaction between HOI and H_2O_2 is a second-order process. The species-specific second order rate constants for the reactions of H_2O_2 with HOI, HO_2^- with HOI, HO_2^- with OI^- are $k_{\text{H}_2\text{O}_2+\text{HOI}} = 29 \pm 5.2 \text{ M}^{-1}\text{s}^{-1}$, $k_{\text{HO}_2^-+\text{HOI}} = (3.1 \pm 0.3) \times 10^8 \text{ M}^{-1} \text{ s}^{-1}$, and $k_{\text{HO}_2^-+\text{OI}^-} = (6.4 \pm 1.4) \times 10^7 \text{ M}^{-1}\text{s}^{-1}$, respectively.
- Phosphate (1.25–25 mM) and acetate (1–25 mM) buffers lead to a significant enhancement of the H_2O_2 –HOI reactivity at pH 7.3 by a factor of 4 and at pH 4.7 by a factor of 3, respectively.

Meanwhile, borate (0.5–25 mM) buffer showed a moderate effect (a factor of 2) on the H_2O_2 –HOI reactivity at pH 9.0.

- The activation energy for the reaction between HOI and H_2O_2 is $E_a = 34 \text{ kJ mol}^{-1}$.
- The formation of I-DBPs in a model system could be significantly reduced by addition of relatively low concentrations of H_2O_2 to HOI- and phenol-containing solutions.
- The species-specific second order rate constants for the reactions of HO_2^- with HOX increased in the order of $\text{HOCl} < \text{HOI} < \text{HOBr}$.
- Oxidative water treatment of iodide-containing water in presence of H_2O_2 can lead to a reduced formation of I-DBPs by minimizing the lifetime of HOI. However, due to the remaining I^- , H_2O_2 based pre-oxidation (e.g., UV/ H_2O_2), followed by chlorination or chloramination may still have a risk of I-DBP formation.
- O_3 deposition by the oxidation of I^- on the seawater surface can be significantly enhanced in presence of H_2O_2 .

Declaration of competing interest

The authors declare that they have no known competing financial interests or personal relationships that could have appeared to influence the work reported in this paper.

Acknowledgements

This study was supported by the École Polytechnique Fédérale de Lausanne (EPFL). The authors thank Caroline Gachet-Acquillon, Eva M.Rodríguez, and Florian Breider for their help in the laboratory, Sebastien Allard and Juan Li for discussions on iodine chemistry, and Michèle Heeb for assistance with the stopped-flow experiments.

Appendix A. Supplementary data

Supplementary data to this article can be found online at <https://doi.org/10.1016/j.watres.2020.115852>.

References

- Allard, S., Tan, J., Joll, C.A., von Gunten, U., 2015. Mechanistic study on the formation of Cl⁻/Br⁻/I⁻ trihalomethanes during chlorination/chloramination combined with a theoretical cytotoxicity evaluation. *Environ. Sci. Technol.* 49, 11105–11114. <https://doi.org/10.1021/acs.est.5b02624>.
- Awad, M.I., Oritani, T., Ohsaka, T., 2003. Kinetic studies on the oxidation of iodide by peroxyacetic acid. *Inorganica Chim. Acta* 344, 253–256. [https://doi.org/10.1016/S0020-1693\(02\)01337-3](https://doi.org/10.1016/S0020-1693(02)01337-3).
- Bader, H., Sturzenegger, V., Hoigné, J., 1988. Photometric method for the determination of low concentrations of hydrogen peroxide by the peroxidase catalyzed oxidation of N,N-diethyl-p-phenylenediamine (DPD). *Water Res.* 22, 1109–1115. [https://doi.org/10.1016/0043-1354\(88\)90005-X](https://doi.org/10.1016/0043-1354(88)90005-X).
- Ball, J.M., Hnatiw, J.B., 2001. The reduction of I_2 by H_2O_2 in aqueous solution. *Can. J. Chem.* 79, 304–311. <https://doi.org/10.1139/v01-027>.
- Bichsel, Y., von Gunten, U., 1999. Oxidation of iodide and hypiodous acid in the disinfection of natural waters. *Environ. Sci. Technol.* 33, 4040–4045. <https://doi.org/10.1021/es990336c>.
- Bichsel, Y., von Gunten, U., 2000a. Formation of iodo-trihalomethanes during disinfection and oxidation of iodide-containing waters. *Environ. Sci. Technol.* 34, 2784–2791. <https://doi.org/10.1021/es9914590>.
- Bichsel, Y., von Gunten, U., 2000b. Hypiodous acid: kinetics of the buffer-catalyzed disproportionation. *Water Res.* 34, 3197–3203. [https://doi.org/10.1016/S0043-1354\(00\)00077-4](https://doi.org/10.1016/S0043-1354(00)00077-4).
- Bray, W.C., Liebafsky, H.A., 1931. Reactions involving hydrogen peroxide, iodine and iodate ion. I. Introduction. *J. Am. Chem. Soc.* 53, 38–44. <https://doi.org/10.1021/ja01352a006>.
- Burger, J.D., Liebafsky, H.A., 1973. Thermodynamic data for aqueous iodine solutions at various temperatures. *Exercise in analytical chemistry. Anal. Chem.* 45, 600–602.
- Bürgi, H., Schaffner, Th, Seiler, J.P., 2001. The toxicology of iodate: a review of the literature. *Thyroid* 11, 449–456. <https://doi.org/10.1089/105072501300176408>.
- Carpenter, L., MacDonald, S., Shaw, M., Kumar, R., Saunders, R., Parthipan, R., Wilson, J., Plane, J., 2013. Atmospheric iodine levels influenced by sea surface emissions of inorganic iodine. *Nat. Geosci.* 6, 108–111. <https://doi.org/10.1038/ngeo1687>.
- Chance, R., Baker, A.R., Carpenter, L., Jickells, T.D., 2014. The distribution of iodide at the sea surface. *Env. Sci. Process. Impacts* 16, 1841–1859. <https://doi.org/10.1039/C4EM00139G>.
- Chang, W., Heikes, B.G., Lee, M., 2004. Ozone deposition to the sea surface: chemical enhancement and wind speed dependence. *Atmos. Environ.* 38, 1053–1059. <https://doi.org/10.1016/j.atmosenv.2003.10.050>.
- Costello, M.J., Cheung, A., De Hauwere, N., 2010. Surface area and the seabed area, volume, depth, slope, and topographic variation for the world's seas, oceans, and countries. *Environ. Sci. Technol.* 44, 8821–8828. <https://doi.org/10.1021/es1012752>.
- Criquet, J., Allard, S., Salhi, E., Joll, C.A., Heitz, A., von Gunten, U., 2012. Iodate and iodo-trihalomethane formation during chlorination of iodide-containing waters: role of bromide. *Environ. Sci. Technol.* 46, 7350–7357. <https://doi.org/10.1021/es301301g>.
- Dong, H., Qiang, Z., Richardson, S.D., 2019. Formation of iodinated disinfection byproducts (I-DBPs) in drinking water: emerging concerns and current issues. *Acc. Chem. Res.* 52, 896–905. <https://doi.org/10.1021/acs.accounts.8b00641>.
- Elliot, A.J., 1992. A pulse radiolysis study of the reaction of OH with I_2 and the decay of I_2^- . *Can. J. Chem.* 70, 1658–1661. <https://doi.org/10.1139/v92-207>.
- Ellison, D.H., Salmon, G.A., Wilkinson, F., 1972. Nanosecond pulse radiolysis of methanolic and aqueous solutions of readily oxidizable solutes. *Proc. R. Soc. Math. Phys. Eng. Sci.* 328, 23–36. <https://doi.org/10.1098/rspa.1972.0066>.
- Furrow, S., 1987. Reactions of iodine intermediates in iodate-hydrogen peroxide oscillators. *J. Phys. Chem.* 91, 2129–2135. <https://doi.org/10.1021/j100292a031>.
- Ganzeveld, L., Helmig, D., Fairall, C.W., Hare, J., Pozzer, A., 2009. Atmosphere-ocean ozone exchange: a global modeling study of biogeochemical, atmospheric, and waterside turbulence dependencies: global oceanic ozone deposition. *Global Biogeochem. Cycles* 23, 1–16. <https://doi.org/10.1029/2008GB003301>.
- Goldberg, R.N., Kishore, N., Lennen, R.M., 2002. Thermodynamic quantities for the ionization reactions of buffers. *J. Phys. Chem. Ref. Data* 31, 231–370. <https://doi.org/10.1063/1.1416902>.
- Gong, T., Zhang, X., 2015. Detection, identification and formation of new iodinated disinfection byproducts in chlorinated saline wastewater effluents. *Water Res.* 68, 77–86. <https://doi.org/10.1016/j.watres.2014.09.041>.
- Hansson, R.C., Henderson, M.J., Jack, P., Taylor, R.D., 1987. Iodoform taste complaints in chloramination. *Water Res.* 21, 1265–1271. [https://doi.org/10.1016/0043-1354\(87\)90179-5](https://doi.org/10.1016/0043-1354(87)90179-5).
- Heeb, M.B., Criquet, J., Zimmermann-Steffens, S.G., von Gunten, U., 2014. Oxidative treatment of bromide-containing waters: formation of bromine and its reactions with inorganic and organic compounds - a critical review. *Water Res.* 48, 15–42. <https://doi.org/10.1016/j.watres.2013.08.030>.
- Held, A.M., Halko, D.J., Hurst, J.K., 1978. Mechanisms of chlorine oxidation of hydrogen peroxide. *J. Am. Chem. Soc.* 100, 5732–5740. <https://doi.org/10.1021/ja00486a025>.
- Helmig, D., Lang, E.K., Bariteau, L., Boylan, P., Fairall, C.W., Ganzeveld, L., Hare, J.E., Hueber, J., Pallandt, M., 2012. Atmosphere-ocean ozone fluxes during the Tex-AQS 2006, STRATUS 2006, GOMECC 2007, GasEx 2008, and AMMA 2008 cruises: atmosphere-ocean ozone fluxes. *J. Geophys. Res. Atmospheres* 117. <https://doi.org/10.1029/2011JD015955> n/a-n/a.
- Ianni, J.C., 2017. Kintecus, windows version 6.01. www.kintecus.com.
- Ishigure, K., Shiraiishi, H., Okuda, H., Fujita, N., 1986. Effect of radiation on chemical forms of iodine species in relation to nuclear reactor accidents. *Int. J. Radiat. Appl. Instrum. C Radiat. Phys. Chem.* 28, 601–610. [https://doi.org/10.1016/1359-0197\(86\)90198-0](https://doi.org/10.1016/1359-0197(86)90198-0).
- Krasner, S.W., Weinberg, H.S., Richardson, S.D., Pastor, S.J., Chinn, R., Scimenti, M.J., Onstad, G.D., Thurston, A.D., 2006. Occurrence of a new generation of disinfection byproducts. *Environ. Sci. Technol.* 40, 7175–7185. <https://doi.org/10.1021/es060353j>.
- Kumar, K., Margerum, D.W., 1987. Kinetics and mechanism of general-acid-assisted oxidation of bromide by hypochlorite and hypochlorous acid. *Inorg. Chem.* 26, 2706–2711. <https://doi.org/10.1021/ic00263a030>.
- Lee, Y., Kissner, R., von Gunten, U., 2014. Reaction of ferrate(VI) with ABTS and self-decay of ferrate(VI): kinetics and mechanisms. *Environ. Sci. Technol.* 48, 5154–5162. <https://doi.org/10.1021/es500804g>.
- Li, J., Jiang, J., Zhou, Y., Pang, S.-Y., Gao, Y., Jiang, C., Ma, J., Jin, Y., Yang, Y., Liu, G., Wang, L., Guan, C., 2017. Kinetics of oxidation of iodide (I^-) and hypiodous acid (HOI) by Peroxymonosulfate (PMS) and formation of iodinated products in the PMS/I⁻/NOM system. *Environ. Sci. Technol. Lett.* 4, 76–82. <https://doi.org/10.1021/acs.estlett.6b00471>.
- Lide, D.R., 2006. *CRC Handbook of Chemistry and Physics: a Ready-Reference Book of Chemical and Physical Data*, 87th ed. CRC, Taylor & Francis.
- Liebafsky, H.A., 1932. The catalytic decomposition of hydrogen peroxide by the iodine-iodide couple at 25°. *J. Am. Chem. Soc.* 54, 1792–1806. <https://doi.org/10.1021/ja01344a011>.
- Luukkonen, T., Pehkonen, S.O., 2017. Peracids in water treatment: a critical review. *Crit. Rev. Environ. Sci. Technol.* 47, 1–39. <https://doi.org/10.1080/10643389.2016.1272343>.
- Moore, C.A., Farmer, C.T., Zika, R.G., 1993. Influence of the Orinoco River on hydrogen peroxide distribution and production in the eastern Caribbean. *J. Geophys. Res. Oceans* 98, 2289–2298. <https://doi.org/10.1029/92JC02767>.
- Moran, J.E., Oktay, S.D., Santschi, P.H., 2002. Sources of iodine and iodine 129 in rivers. *Water Resour. Res.* 38. <https://doi.org/10.1029/2001WR000622>, 24-1–24–10.

- Nagarajan, V., Fessenden, R.W., 1985. Flash photolysis of transient radicals. 1. X2- with X = Cl, Br, I, and SCN. *J. Phys. Chem.* 89, 2330–2335. <https://doi.org/10.1021/j100257a037>.
- Nagy, J.C., Kumar, K., Margerum, D.W., 1988. Nonmetal redox kinetics: oxidation of iodide by hypochlorous acid and by nitrogen trichloride measured by the pulsed-accelerated-flow method. *Inorg. Chem.* 27, 2773–2780. <https://doi.org/10.1021/ic00289a007>.
- Önnby, L., Salhi, E., McKay, G., Rosario-Ortiz, F.L., von Gunten, U., 2018. Ozone and chlorine reactions with dissolved organic matter - assessment of oxidant-reactive moieties by optical measurements and the electron donating capacities. *Water Res.* 144, 64–75. <https://doi.org/10.1016/j.watres.2018.06.059>.
- Pan, Y., Li, W., An, H., Cui, H., Wang, Y., 2016. Formation and occurrence of new polar iodinated disinfection byproducts in drinking water. *Chemosphere* 144, 2312–2320. <https://doi.org/10.1016/j.chemosphere.2015.11.012>.
- Pillar, E.A., Guzman, M.I., Rodriguez, J.M., 2013. Conversion of iodide to hypoiodous acid and iodine in aqueous microdroplets exposed to ozone. *Environ. Sci. Technol.* 47, 10971–10979. <https://doi.org/10.1021/es401700h>.
- Pinkernell, U., Nowack, B., Gallard, H., von Gunten, U., 2000. Methods for the photometric determination of reactive bromine and chlorine species with ABTS. *Water Res.* 34, 4343–4350. [https://doi.org/10.1016/S0043-1354\(00\)00216-5](https://doi.org/10.1016/S0043-1354(00)00216-5).
- Pinkernell, U., von Gunten, U., 2001. Bromate minimization during ozonation: mechanistic considerations. *Environ. Sci. Technol.* 35, 2525–2531. <https://doi.org/10.1021/es001502f>.
- Plewa, M.J., Wagner, E.D., Richardson, S.D., Thruston, A.D., Woo, Y.-T., McKague, A.B., 2004. Chemical and biological characterization of newly discovered iodoacid drinking water disinfection byproducts. *Environ. Sci. Technol.* 38, 4713–4722. <https://doi.org/10.1021/es049971v>.
- Price, D., Mantoura, R.F.C., Worsfold, P.J., 1998. Shipboard determination of hydrogen peroxide in the western Mediterranean sea using flow injection with chemiluminescence detection. *Anal. Chim. Acta* 377, 145–155. [https://doi.org/10.1016/S0003-2670\(98\)00621-7](https://doi.org/10.1016/S0003-2670(98)00621-7).
- Richardson, S.D., Fasano, F., Ellington, J.J., Crumley, F.G., Buettner, K.M., Evans, J.J., Blount, B.C., Silva, L.K., Waite, T.J., Luther, G.W., McKague, A.B., Miltner, R.J., Wagner, E.D., Plewa, M.J., 2008. Occurrence and mammalian cell toxicity of iodinated disinfection byproducts in drinking water. *Environ. Sci. Technol.* 42, 8330–8338. <https://doi.org/10.1021/es801169k>.
- Sarwar, G., Gantt, B., Schwede, D., Foley, K., Mathur, R., Saiz-Lopez, A., 2015. Impact of enhanced ozone deposition and halogen chemistry on tropospheric ozone over the Northern Hemisphere. *Environ. Sci. Technol.* 49, 9203–9211. <https://doi.org/10.1021/acs.est.5b01657>.
- Schmitz, G., 2010. Iodine oxidation by hydrogen peroxide in acidic solutions, Bray-Liebafsky reaction and other related reactions. *Phys. Chem. Chem. Phys.* 12, 6605. <https://doi.org/10.1039/b927432d>.
- Shah, A.D., Liu, Z.-Q., Salhi, E., Höfer, T., von Gunten, U., 2015a. Peracetic acid oxidation of saline waters in the absence and presence of H₂O₂: secondary oxidant and disinfection byproduct formation. *Environ. Sci. Technol.* 49, 1698–1705. <https://doi.org/10.1021/es503920n>.
- Shah, A.D., Liu, Z.-Q., Salhi, E., Höfer, T., Werschkun, B., von Gunten, U., 2015b. Formation of disinfection by-products during ballast water treatment with ozone, chlorine, and peracetic acid: influence of water quality parameters. *Environ. Sci. Water Res. Technol.* 1, 465–480. <https://doi.org/10.1039/C5EW00061K>.
- Shin, J., von Gunten, U., Reckhow, D.A., Allard, S., Lee, Y., 2018. Reactions of ferrate(VI) with iodide and hypoiodous acid: kinetics, pathways, and implications for the fate of iodine during water treatment. *Environ. Sci. Technol.* 52, 7458–7467. <https://doi.org/10.1021/acs.est.8b01565>.
- Shiraishi, H., Okuda, H., Morinago, Y., Ishigure, K., 1992. Measurement on the rate of some reactions relevant to iodine chemistry in the aqueous phase. In: Ishigure, K., Saeki, M., Soda, K., Sigimoto, J. (Eds.), *Proceedings of the Third CSNI Workshop on Iodine Chemistry in Reactor Safety*. Japan Atomic Energy Research Institute, Tokaimuri, Japan, pp. 152–162, 1992.
- Simpson, W.R., Brown, S.S., Saiz-Lopez, A., Thornton, J.A., von Glasow, R., 2015. Tropospheric halogen chemistry: sources, cycling, and impacts. *Chem. Rev.* 115, 4035–4062. <https://doi.org/10.1021/cr5006638>.
- Smedley, P., 2000. *Water Quality Fact Sheet: Iodine*. British Geological Survey, Nottingham, UK.
- Soltermann, F., Abegglen, C., Tschui, M., Stahel, S., von Gunten, U., 2017. Options and limitations for bromate control during ozonation of wastewater. *Water Res.* 116, 76–85. <https://doi.org/10.1016/j.watres.2017.02.026>.
- Stahelin, J., Hoigné, J., 1982. Decomposition of ozone in water: rate of initiation by hydroxide ions and hydrogen peroxide. *Environ. Sci. Technol.* 16, 676–681. <https://doi.org/10.1021/es00104a009>.
- Stefan, M.I., 2017. Advanced oxidation processes for water treatment - fundamentals and applications. *Water Intell. Online* 16. https://doi.org/10.2166/9781780407197_9781780407197.
- von Gunten, U., Oliveras, Y., 1997. Kinetics of the reaction between hydrogen peroxide and hypobromous acid: implication on water treatment and natural systems. *Water Res.* 31, 900–906. [https://doi.org/10.1016/S0043-1354\(96\)00368-5](https://doi.org/10.1016/S0043-1354(96)00368-5).
- von Gunten, U., Oliveras, Y., 1998. Advanced oxidation of bromide-containing waters: bromate formation mechanisms. *Environ. Sci. Technol.* 32, 63–70. <https://doi.org/10.1021/es970477j>.
- von Sonntag, C., von Gunten, U., 2012. *Chemistry of ozone in water and wastewater treatment: from basic principles to applications*. IWA Publ., London.
- Wang, X., Liu, Y., Huang, Z., Wang, L., Wang, Y., Li, Y., Li, J., Qi, J., Ma, J., 2018. Rapid oxidation of iodide and hypoiodous acid with ferrate and no formation of iodoform and monoiodoacetic acid in the ferrate/I⁻/HA system. *Water Res.* 144, 592–602. <https://doi.org/10.1016/j.watres.2018.07.061>.
- Wei, X., Chen, X., Wang, X., Zheng, W., Zhang, D., Tian, D., Jiang, S., Ong, C.N., He, G., Qu, W., 2013. Occurrence of regulated and emerging iodinated DBPs in the Shanghai drinking water. *PLoS One* 8, e59677. <https://doi.org/10.1371/journal.pone.0059677>.
- Werschkun, B., Banerji, S., Basurko, O.C., David, M., Fuhr, F., Gollasch, S., Grummt, T., Haerich, M., Jha, A.N., Kacan, S., Kehrer, A., Linders, J., Mesbahi, E., Pughic, D., Richardson, S.D., Schwarz-Schulz, B., Shah, A., Theobald, N., von Gunten, U., Wieck, S., Höfer, T., 2014. Emerging risks from ballast water treatment: the run-up to the international ballast water management convention. *Chemosphere* 112, 256–266. <https://doi.org/10.1016/j.chemosphere.2014.03.135>.
- Yang, Y., Komaki, Y., Kimura, S.Y., Hu, H.-Y., Wagner, E.D., Mariñas, B.J., Plewa, M.J., 2014. Toxic impact of bromide and iodide on drinking water disinfected with chlorine or chloramines. *Environ. Sci. Technol.* 48, 12362–12369. <https://doi.org/10.1021/es503621e>.
- Zhang, J., Liu, J., He, C.-S., Qian, C., Mu, Y., 2018. Formation of iodo-trihalomethanes (I-THMs) during disinfection with chlorine or chloramine: impact of UV/H₂O₂ pre-oxidation. *Sci. Total Environ.* 640–641, 764–771. <https://doi.org/10.1016/j.scitotenv.2018.05.306>.
- Zhao, X., Ma, J., von Gunten, U., 2017. Reactions of hypoiodous acid with model compounds and the formation of iodoform in absence/presence of permanganate. *Water Res.* 119, 126–135. <https://doi.org/10.1016/j.watres.2017.04.033>.
- Zhao, X., Salhi, E., Liu, H., Ma, J., von Gunten, U., 2016. Kinetic and mechanistic aspects of the reactions of iodide and hypoiodous acid with permanganate: oxidation and disproportionation. *Environ. Sci. Technol.* 50, 4358–4365. <https://doi.org/10.1021/acs.est.6b00320>.
- Zika, R.G., Moffett, J.W., Petasne, R.G., Cooper, W.J., Saltzman, E.S., 1985. Spatial and temporal variations of hydrogen peroxide in Gulf of Mexico waters. *Geochim. Cosmochim. Acta* 49, 1173–1184. [https://doi.org/10.1016/0016-7037\(85\)90008-0](https://doi.org/10.1016/0016-7037(85)90008-0).